Nonisolated Two-Channel LED Driver With Automatic Current Balance and Zero-Voltage Switching

K. I. Hwu, *Member, IEEE*, and W. Z. Jiang, *Student Member, IEEE*

***Abstract*—In this paper, a nonisolated two-channel light-emitting diode (LED) driver with automatic current balance and zero-voltage switching (ZVS) is presented. In this LED driver, a dc-blocking capacitor is connected with one side of the coupled inductor. Therefore, based on the ampere–second balance, a current source is generated with the average value of the positive current identical to the absolute average value of the negative current. Accordingly, the LED currents can be balanced naturally without extra active components or current sharing transformer. Consequently, the circuit components can keep at a low count. In addition, the proposed LED driver can achieve ZVS turn-on. Thus, the switching loss can be decreased. Above all, the proposed two-channel LED driver can be extended to a multichannel LED driver. In this paper, detailed theoretical analyses and experimental results are provided to verify the feasibility and effectiveness of the proposed LED driver.**

***Index Terms*—Automatic current balance, coupled inductor, dc blocking capacitor, light-emitting diode (LED) driver, zero-voltage switching (ZVS).**

I. Introduction

NOWADAYS, the light-emitting diode (LED) has been widely used due to its long life, small size, and environmental friendly characteristics [1], [2]. Due to the fact that the brightness of the LEDs is proportional to the LED current, it is preferable to use the constant current control. Moreover, since the LED strings are usually formed by connecting them in series and parallel, to obtain uniform brightness, the current in each LED string should be equally distributed. Furthermore, due to the negative temperature coefficient of an LED and different manufacturing tolerance in *V–I* characteristics, it is necessary to achieve current balance by using current sharing technique.

Until now, there are many methods which have been proposed to achieve current balance in LEDs. They can be categorized into two types. One is the active method [3]–[6], and the other is the passive method [7]–[22]. Due to the fact that the passive method features low cost and simple structure [18], [22], the passive methods have been regarded as a solution for achieving current balancing in LED strings. The passive balancing methods can be divided into the inductive method [7]–[11] and the capacitive method [12]–[21]. In [7]–[11], the current sharing transformer is employed to achieve the current balancing among LED strings. However, this method suffers from some problems. First, due to the use of the magnetic components, the size is bulky. Second, the LED current balance performance is influenced by the coupling coefficient and the LED forward voltage tolerance. Third, the magnetizing and leakage inductors of the current sharing transformer should be reset during the switch turn-off period. Otherwise, it will result in high-voltage spikes. Therefore, it should be careful to design the LED driver using the current sharing transformer. In [12], the current balancing is realized by connecting the identical capacitors in series with the individual LED. However, the current balancing performance is affected by the capacitance tolerance. In [13]–[19], a dc blocking capacitor is connected with the secondary-side winding of the transformer and based on the charge balancing principle of capacitor, the currents in the LED strings can be automatically balanced. For the main power structure, the full bridge and half-bridge topologies are used to generate an ac current source. This method features simple structure, low cost, and precise current balance. Thus, the LED current balancing using this method is getting more and more attention. However, the structures in [13]–[19] are more suitable for high input voltage applications. In [20], the capacitor-clamped current sharing circuit is presented. By using the interleaved control of the LED control switches, the current balancing in LEDs can be realized. Moreover, such a method can be applied to the isolated and nonisolated applications. However, this method needs additional switches and control drivers, and leads to complexity and high cost. In [21], a nonisolated low power LED driver is proposed. This LED driver features a simple structure for low power LEDs. However, if two LED strings are connected in parallel, an additional current balancing circuit is needed, thereby resulting in complexity.

In this paper, in order to overcome the above problems, a two-channel nonisolated LED driver with a simple structure and low cost is presented. The proposed LED driver is based on the structure in [22]. The converter in [22] is a bidirectional converter, which can operate at a step-down mode and a step-up mode. Since there is a dc-blocking capacitor connected in the primary side of the coupled inductor, the step-down gain and step-up gain can be much higher. From [22], it can be seen that due to the use of the dc-blocking capacitor, the charge and discharge quantity over one cycle is equal. Therefore, the average current of $i_{C1}(+)$ is identical to the average current of $i_{C1}(-)$.

Manuscript received October 14, 2015; revised December 23, 2015; accepted December 30, 2015. Date of publication January 06, 2016; date of current version July 08, 2016. This work was supported by the Ministry of Science and Technology under Grant MOST 103-2221-E-027-040-MY3. Recommended for publication by Associate Editor J. M. Alonso.

The authors are with the Department of Electrical Engineering, National Taipei University of Technology, Taipei 10608, Taiwan (e-mail: eaglehwu@ntut.edu.tw; newjerusalem333@gmail.com).

Color versions of one or more of the figures in this paper are available online at http://ieeexplore.ieee.org.

Digital Object Identifier 10.1109/TPEL.2016.2515088

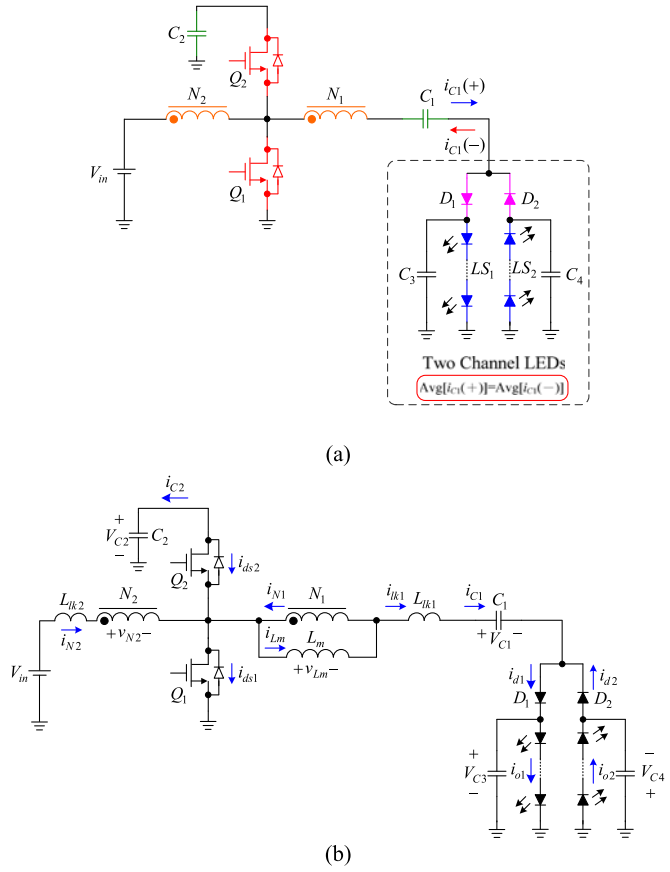

Fig. 1. Proposed two-channel LED driver: (a) main structure, (b) equivalent circuit model.

Hence, the proposed nonisolated two-channel LED driver is based on this concept, and the currents in two LED strings can be balanced naturally without any additional active and passive components, such as switch, current sharing controller, current sharing transformer, etc. By replacing the two LED strings with the high-voltage side of the bidirectional converter, the proposed nonisolated two-channel LED driver is shown in Fig. 1(a). In the proposed LED driver, there are some advantages. First, due to the dc-blocking capacitor, the two LED currents can be balanced automatically. Second, due to the combination of the dc-blocking capacitor and the coupled inductor, a high-output voltage gain can be achieved. The voltage gain contains the parameters of not only the duty cycle but also the turns ratio. Thus, there are two degrees of freedom to tune the voltage gain in design. Third, the voltage spike from the leakage inductance of the coupled inductor can be recycled to the capacitor C_2 so that low-voltage MOSFETs can be used. Furthermore, the two switches can be driven by using only one half-bridge driver, so no isolated driver is required. Therefore, the proposed nonisolated two-channel LED driver is simple and easy to design and control. Moreover, the proposed two-channel LED driver can be extended to a multichannel LED driver. It should be noticed that due to the use of a coupled inductor, the actual voltage will be influenced by the leakage inductance. Moreover, similar to other coupled-inductor-based converters, one of the windings of the coupled inductor is connected to the input terminal, and hence the input current is pulsating, whose peak-to-peak value

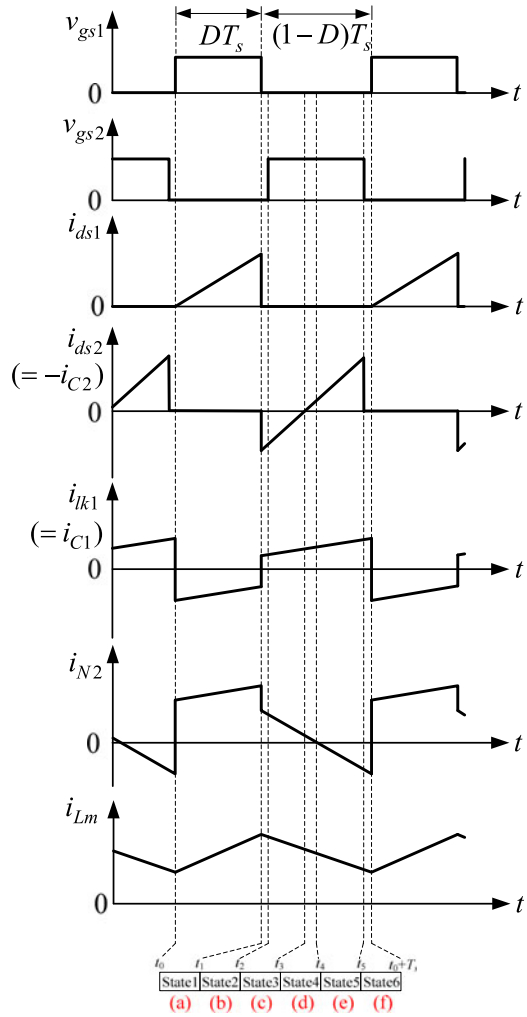

Fig. 2. Illustrated waveforms of the proposed two-channel LED driver.

depends on the turns ratio as well as the input voltage and the load. On the other hand, for the step-up converters, the voltage gain is limited by the parasitic components, i.e., if the duty cycle approaches to 1, the real output voltage will drop sharply [23]. Based on the aforementioned, the tradeoff between turns ratio and duty cycle should be taken into account.

II. Basic Analysis of the Proposed LED Driver

Fig. 1(a) shows the proposed two-channel LED driver, which contains a half-bridge switch Q_1 and Q_2, one coupled inductor composed of the primary winding N_1 and the secondary winding N_2, two energy-transferring capacitors C_1 and C_2, two output diodes D_1 and D_2, two output capacitors C_3 and C_4, and two LED strings LS_1 and LS_2.

The equivalent circuit of the proposed converter is shown in Fig. 1(b). The coupled inductor is modeled as an ideal transformer with a primary winding N_1 and a secondary winding N_2 connected in series with a leakage inductor L_{lk2}, a magnetizing inductor L_m connected in parallel with N_1, and a leakage inductor L_{lk1}.

Moreover, the currents flowing through Q_1, Q_2, C_1, C_2, N_1, N_2, L_m, D_1, D_2, LS_1, and LS_2 are signified by $i_{ds1}, i_{ds2}, i_{C1}, i_{C2}, i_{N1}, i_{N2}, i_{Lm}, i_{d1}, i_{d2}, i_{o1}$, and i_{o2},

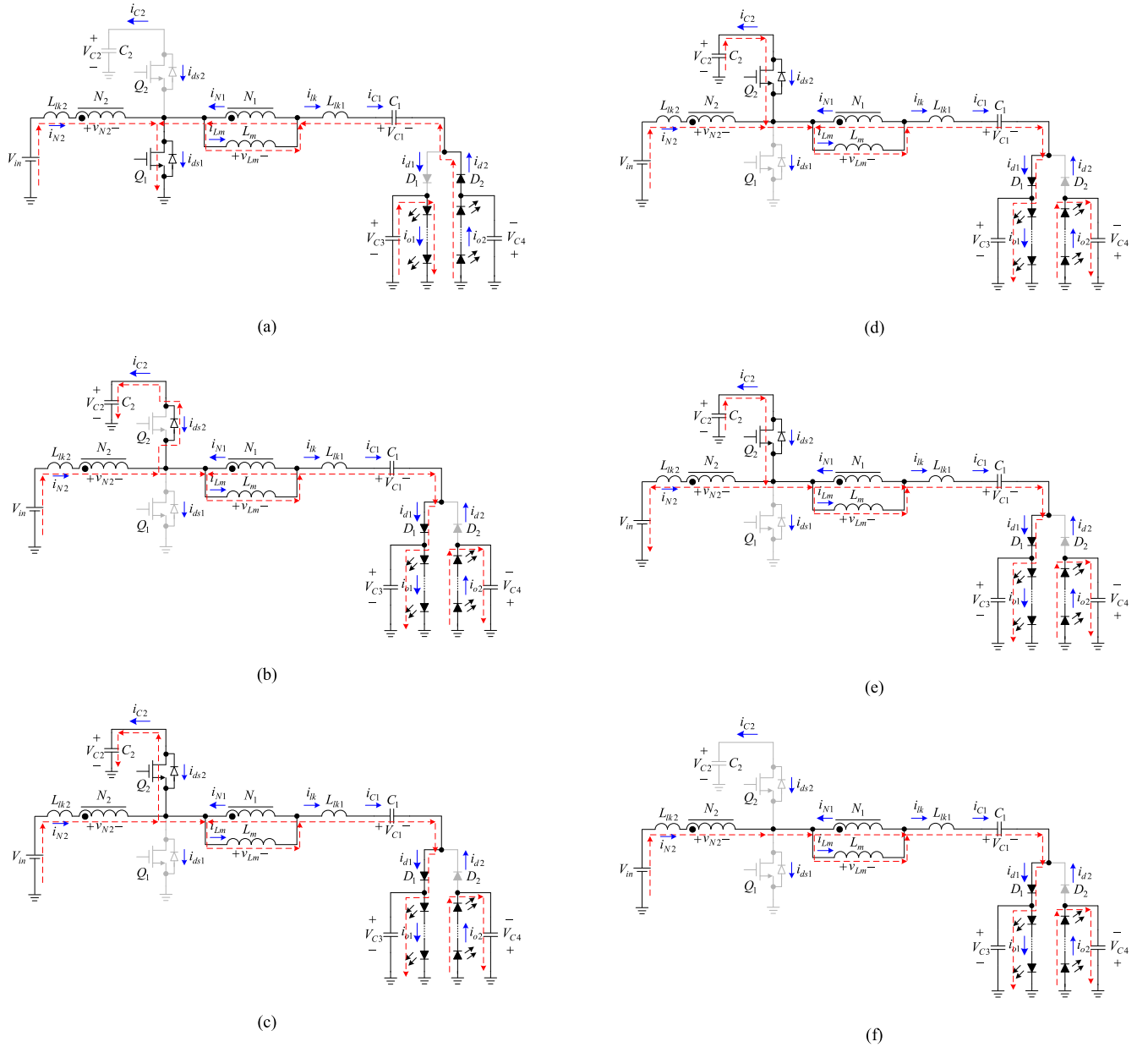

Fig. 3. Operating circuits over one switching period: (a) state 1, (b) state 2, (c) state 3, (d) state 4, (e) state 5, (f) state 6.

respectively. The voltage across L_m or the N_1 winding is signified by v_{Lm}, the voltage across the N_2 winding is represented by v_{N2}, the voltages across C_1, C_2, C_3, and C_4 are indicated by $V_{\mathrm{C1}}, V_{\mathrm{C2}}, V_{\mathrm{C3}}$, and V_{C4}, respectively. In addition, the gate driving signal for the switch Q_1 has the duty cycle of D, and the gate driving signal for the switch Q_2 has the duty cycle of $(1-D)$, which is complementary to Q_1.

Besides, in order to make the analysis of the proposed converter easier, there are some assumptions to be made as follows:

1) all the switches and components are assumed to be ideal;
2) the values of all the capacitors are large enough. Thus, the voltages are regarded to be constant.

The following analyses contain operating principles, voltage gain, boundary condition of the magnetizing inductor current, automatic current sharing, and multichannel extension.

A. Operating Principles

There are six operating states to be described below. Fig. 2 shows the illustrated waveforms over one switching period.

1) *State 1 [t_0, t_1]:* As shown in Fig. 3(a), Q_1 is turned ON, but Q_2 is in the off-state. During this state, the voltage

$$V_{\mathrm{in}} \cdot \frac{L_m\left(\frac{\mathrm{N}_2}{\mathrm{N}_1}\right)}{L_{\mathrm{lk2}} + L_m\left(\frac{\mathrm{N}_2}{\mathrm{N}_1}\right)^2}$$

is imposed on L_m. Thus, i_{Lm} is increasing linearly. Meanwhile, C_1 is discharged, so i_{C1} or i_{lk1} is increasing in the opposite direction. Moreover, D_1 is reverse-biased, but D_2 is forward-biased. Hence, the LED string LS_1 is supplied by C_3, whereas the LED string LS_2 is supplied by i_{lk} in

the opposite direction. This state ends when Q_1 is turned OFF at t_1.

2) *State 2 [t_1, t_2]:* As shown in Fig. 3(b), the switch Q_1 becomes turned OFF, and the switch Q_2 still keeps turned OFF. During this state, the voltage $V_{\rm in} - V_{\rm C2}$, which is a negative voltage, is imposed on $L_{\rm lk2}$ and L_m. Thus, $i_{\rm Lm}$ begins to decrease linearly. During this blanking time, the body diode of the switch Q_2 is forward-biased. Moreover, D_1 is forward-biased, but D_2 is reverse-biased. Hence, the LED string LS_1 is supplied by $i_{\rm lk}$, whereas the LED string LS_2 is supplied by C_4. This state ends when Q_2 is turned ON at $t = t_2$.
3) *State 3 [t_2, t_3]:* Before the state 3 begins, the body diode of the switch Q_2 is conducted. Thus, Q_2 is turned ON with zero-voltage switching (ZVS) as shown in Fig. 3(c), but Q_1 still keeps turned OFF. $i_{\rm Lm}$ is continuously decreasing. Also, the behavior of two LED strings is the same as that in state 2. Once $i_{\rm N2}$ is equal to $i_{\rm lk1}$, $i_{\rm ds2}$ reaches zero, and this state ends at $t = t_3$.
4) *State 4 [t_3, t_4]:* As shown in Fig. 3(d), the switch Q_1 still keeps turned OFF, but the switch Q_2 still keeps turned ON. During this state, the capacitor C_2 is discharged, and the current $i_{\rm C2}$ begins to increase in the opposite direction. Meanwhile, $i_{\rm lk1}$ is increasing, $i_{\rm N2}$ is decreasing, and $i_{\rm Lm}$ is decreasing. Also, the behavior of two LED strings is the same as that in state 2. This state ends when $i_{\rm N2}$ drops to zero at $t = t_4$.
5) *State 5 [t_4, t_5]:* As shown in Fig. 3(e), the switch Q_1 still keeps turned OFF, and the switch Q_2 still keeps turned ON. During this state, the capacitor C_2 is still discharged, the current $i_{\rm C2}$ is increasing continuously, $i_{\rm N2}$ begins to increase in the opposite direction, and $i_{\rm Lm}$ is decreasing continuously. Also, the behavior of two LED strings is the same as that in state 2. This state ends when Q_2 is turned OFF at $t = t_5$.
6) *State 6 [t_5, $t_0 + T_s$]:* As shown in Fig. 3(f), the switch Q_1 still keeps turned OFF, and the switches Q_2 becomes turned OFF. During this state, the magnetizing inductor is still demagnetized. Thus, $i_{\rm Lm}$ is decreasing continuously. Also, the behavior of two LED strings is the same as that in state 2. This state ends when Q_2 is turned ON at $t = t_0 + T_s$, and the next cycle is repeated.

B. Voltage Gain

Since the effective turns ratio is not equal to the physical turns ratio due to the presence of the leakage flux, in order to calculate the voltage gain, the effect of coupling coefficient should be taken into consideration. From [24], the coupled inductor is modeled as shown in Fig. 4. The ratio of the voltages of the coupled inductor with nonperfect coupling is

$$\frac{v_1}{v_2} = k\sqrt{\frac{L_1}{L_2}} \tag{1}$$

where k is the coupling coefficient, and L_1 and L_2 are the self-inductances of the primary and secondary windings, respectively. Besides, $L_1 = L_{\rm lk1} + L_m$ and $L_2 = L_{\rm lk2} + (\frac{N_2}{N_1})^2 L_m$.

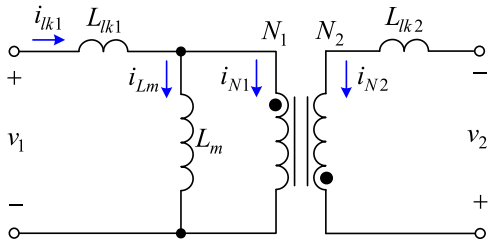

Fig. 4. Equivalent model of the coupled inductor.

In order to obtain the voltage gain and the voltages across C_1 and C_2, only states 1 and 4 are considered, and the dead times are ignored. From state 1 as shown in Fig. 3(a), $v_{\rm Lm}$ and $V_{\rm C1}$ can be found to be

$$v_{\rm Lm} = \frac{L_m\left(\frac{N_2}{N_1}\right)}{L_{\rm lk2} + L_m\left(\frac{N_2}{N_1}\right)^2} \cdot V_{\rm in} \tag{2}$$

$$\begin{aligned} V_{\rm C1} &= V_{\rm C4} - v_1 = V_{\rm C4} - v_2 \cdot k\sqrt{\frac{L_1}{L_2}} \\ &= V_{\rm C4} - V_{\rm in} \cdot k\sqrt{\frac{L_1}{L_2}}. \end{aligned} \tag{3}$$

From state 4 as shown in Fig. 3(d), $v_{\rm Lm}$ and $V_{\rm C3}$ can be found to be

$$v_{\rm Lm} = \frac{L_m\left(\frac{N_2}{N_1}\right)}{L_{\rm lk2} + L_m\left(\frac{N_2}{N_1}\right)^2} \cdot (V_{\rm in} - V_{\rm C2}) \tag{4}$$

$$\begin{aligned} V_{\rm C3} &= V_{\rm C2} - v_1 - V_{\rm C1} \\ &= V_{\rm C2} - (V_{\rm in} - V_{\rm C2}) \cdot k\sqrt{\frac{L_1}{L_2}} - V_{\rm C1} \end{aligned} \tag{5}$$

Based on (2) and (4), and by applying the voltage–second balance in the steady state to L_m over one switching period, the following equation can be obtained:

$$\begin{aligned} &D \cdot \frac{L_m\left(\frac{N_2}{N_1}\right)}{L_{\rm lk2} + L_m\left(\frac{N_2}{N_1}\right)^2} \cdot V_{\rm in} + (1-D) \\ &\quad \cdot \frac{L_m\left(\frac{N_2}{N_1}\right)}{L_{\rm lk2} + L_m\left(\frac{N_2}{N_1}\right)^2} \cdot (V_{\rm in} - V_{\rm C2}) = 0. \end{aligned} \tag{6}$$

By rearranging the above equation, the voltage across C_2 and $V_{\rm C2}$ can be expressed by

$$V_{\rm C2} = \frac{1}{1-D} \cdot V_{\rm in}. \tag{7}$$

Next, based on (3), (5), and (7), the following equation can be obtained:

$$\begin{aligned} V_{\rm C3} &= V_{\rm C2} - (V_{\rm in} - V_{\rm C2}) \cdot k\sqrt{\frac{L_1}{L_2}} - V_{\rm C1} \\ &= V_{\rm C2} \cdot \left(1 + k\sqrt{\frac{L_1}{L_2}}\right) - V_{\rm in} \cdot k\sqrt{\frac{L_1}{L_2}} - V_{\rm C1} \end{aligned}$$

$$= V_{C2} \cdot \left(1 + k\sqrt{\frac{L_1}{L_2}}\right) - V_{in} \cdot k\sqrt{\frac{L_1}{L_2}} - V_{C4} + V_{in} \cdot k\sqrt{\frac{L_1}{L_2}}. \quad (8)$$

By rearranging the above equation, the following equation can be obtained:

$$V_{C3} + V_{C4} = \left(\frac{1 + k\sqrt{\frac{L_1}{L_2}}}{1 - D}\right) \cdot V_{in}. \quad (9)$$

In (9), if the coupled inductor is perfectly coupled, then $L_{lk2} = 0$, $k = 1$, and $(L_1/L_2)^{1/2} = N_1/N_2$. Hence, (9) can be simplified to be

$$V_{C3} + V_{C4} = \frac{1 + \frac{N_1}{N_2}}{1 - D} \cdot V_{in}. \quad (10)$$

From (10), the output voltage of the LED driver is $V_{C3} + V_{C4}$, so the corresponding voltage gain is determined by the duty ratio D, and the turns ratio N_1/N_2 of the coupled inductor.

C. Boundary Condition of Magnetizing Inductor Current

The condition for the output inductor L_m operating in the positive current region or negative current region is described as follows:

$$\begin{cases} 2I_{Lm} \geq \Delta i_{Lm}, \text{positive current region} \\ 2I_{Lm} < \Delta i_{Lm}, \text{negative current region} \end{cases} \quad (11)$$

where I_{Lm} and Δi_{Lm} are the dc component of i_{Lm} and the peak-to-peak value of the ac component of i_{Lm}, respectively.

In the proposed LED driver, the magnetizing inductance current of the coupled inductor can be derived as follows:

$$i_{Lm} = i_{N1} + i_{C1} = \frac{N_2}{N_1} \cdot i_{N2} + i_{C1}. \quad (12)$$

According to the ampere–second balance in the steady state, the averaging value of the current in C_1 is zero. Therefore,

$$\langle i_{Lm} \rangle = \frac{N_2}{N_1} \cdot \langle i_{N2} \rangle + \langle i_{C1} \rangle. \quad (13)$$

The above equation can be rewritten as

$$I_{Lm} = \frac{N_2}{N_1} \cdot I_{N2} \quad (14)$$

where $\langle i_{Lm} \rangle$ or I_{Lm}, $\langle i_{N2} \rangle$ or I_{N2}, and $\langle i_{C1} \rangle$ are the average values of i_{Lm}, i_{N2}, and i_{C1}, respectively.

The efficiency η of the proposed LED can be expressed as

$$\eta = \frac{P_o}{P_{in}} \times 100\%. \quad (15)$$

By substituting the relevant parameters into (15), (15) can be rewritten as

$$\eta = \frac{V_{C3} \cdot I_{o1} + V_{C4} \cdot I_{o2}}{V_{in} \cdot I_{in}} \times 100\%. \quad (16)$$

For the proposed LED driver, the currents in the two LED strings are balanced, and the average value of input current i_{in}, I_{in}, is equal to the average value of i_{N2}, I_{N2}. Hence, (16) can be rewritten to be

$$\eta = \frac{(V_{C3} + V_{C4}) \cdot I_{o1}}{V_{in} \cdot I_{N2}} \times 100\% \quad (17)$$

where I_{o1} and I_{o2} are the average values of i_{o1} and i_{o2}, respectively.

Based on (17), I_{N2} can be represented by

$$I_{N2} = \frac{(V_{C3} + V_{C4})}{V_{in} \cdot \eta} \cdot I_{o1}. \quad (18)$$

Next, by substituting the voltage gain shown in (9) into (18), (18) can be rewritten as

$$I_{N2} = \left(\frac{1 + k\sqrt{\frac{L_1}{L_2}}}{1 - D}\right) \cdot \frac{1}{\eta} \cdot I_{o1}. \quad (19)$$

Substituting (19) into (14) yields the following equation:

$$I_{Lm} = \left(\frac{1 + k\sqrt{\frac{L_1}{L_2}}}{1 - D}\right) \cdot \frac{1}{\eta} \cdot \frac{N_2}{N_1} I_{o1}. \quad (20)$$

Also, Δi_{Lm} can be expressed by

$$\Delta i_{Lm} = \frac{v_{Lm} \Delta t}{L_m} = \frac{\frac{L_m\left(\frac{N_2}{N_1}\right)}{L_{lk2} + L_m\left(\frac{N_2}{N_1}\right)^2} \cdot V_{in} \cdot DT_s}{L_m}. \quad (21)$$

As $2I_{Lm} \geq \Delta i_{Lm}$, I_{Lm} will be always positive. To make sure that I_{Lm} is always positive, the required magnetizing inductance is as follows:

$$\begin{aligned} & 2I_{Lm} \geq \Delta i_{Lm} \\ & \Rightarrow 2 \cdot \left(\frac{1 + k\sqrt{\frac{L_1}{L_2}}}{1 - D}\right) \cdot \frac{1}{\eta} \cdot \frac{N_2}{N_1} \cdot I_{o1} \\ & \quad \geq \frac{\frac{L_m\left(\frac{N_2}{N_1}\right)}{L_{lk2} + L_m\left(\frac{N_2}{N_1}\right)^2} \cdot V_{in} \cdot DT_s}{L_m} \\ & \Rightarrow L_m \geq \frac{\frac{L_m\left(\frac{N_2}{N_1}\right)}{L_{lk2} + L_m\left(\frac{N_2}{N_1}\right)^2} \cdot \frac{N_1}{N_2} \cdot V_{in} \cdot DT_s \cdot \eta}{2 \cdot \left(\frac{1 + k\sqrt{\frac{L_1}{L_2}}}{1 - D}\right) \cdot I_{o1}}. \end{aligned} \quad (22)$$

If the coupled inductor is perfectly coupled, (22) becomes

$$L_m \geq \frac{\frac{N_1}{N_2} \cdot V_{in} \cdot D(1 - D)T_s \cdot \eta}{2\left(1 + \frac{N_2}{N_1}\right) \cdot I_{o1}}. \quad (23)$$

D. Automatic Current Sharing

To analyze the LED current balance, the associated waveforms are shown in Fig. 5. According to the ampere–second

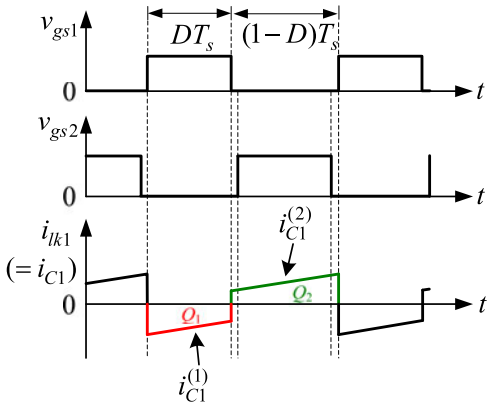

Fig. 5. Waveforms for analyzing the LED current balance.

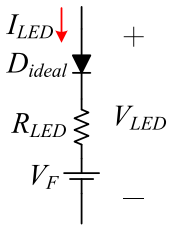

Fig. 6. Approximately linear model of an LED.

balance, the charge Q_1 flowing through C_1 is equal to the charge Q_2 flowing through C_1. Therefore, the following equations can be obtained:

$$|Q_1| = |Q_2| \tag{24}$$

$$\frac{1}{T_s}\int_0^{DT_s}\left|i_{C1}^{(1)}\right|dt = \frac{1}{T_s}\int_{DT_s}^{T_s}\left|i_{C1}^{(2)}\right|dt \tag{25}$$

$$\left|I_{C1}^{(1)}\right| = \left|I_{C1}^{(2)}\right|. \tag{26}$$

The current in the LED string LS_1 is the average value of the negative part of i_{C1}, and the current in the LED string LS_2 is the average value of the positive part of i_{C2}. Therefore

$$I_{o1} = \left|I_{C1}^{(1)}\right| \tag{27}$$

$$I_{o2} = \left|I_{C1}^{(2)}\right|. \tag{28}$$

It is obvious that due to the capacitor C_1, the currents in both LED channels are balanced naturally.

E. Current Regulation

From [25], the LED can be modeled as an approximately linear model as shown in Fig. 6. From Fig. 6, it can be seen that the LED is modeled as an ideal diode D_{ideal}, an on-resistance R_{LED}, and a forward voltage V_F, which are all connected in series. The LED voltage V_{LED} can be expressed as

$$V_{\text{LED}} = R_{\text{LED}} I_{\text{LED}} + V_F. \tag{29}$$

If the LED count in an LED string is k with LEDs identical to each other, the total LED voltage on this LED string is

$$V_{\text{LED},k} = R_{\text{LED},k} I_{\text{LED}} + V_{F,k} \tag{30}$$

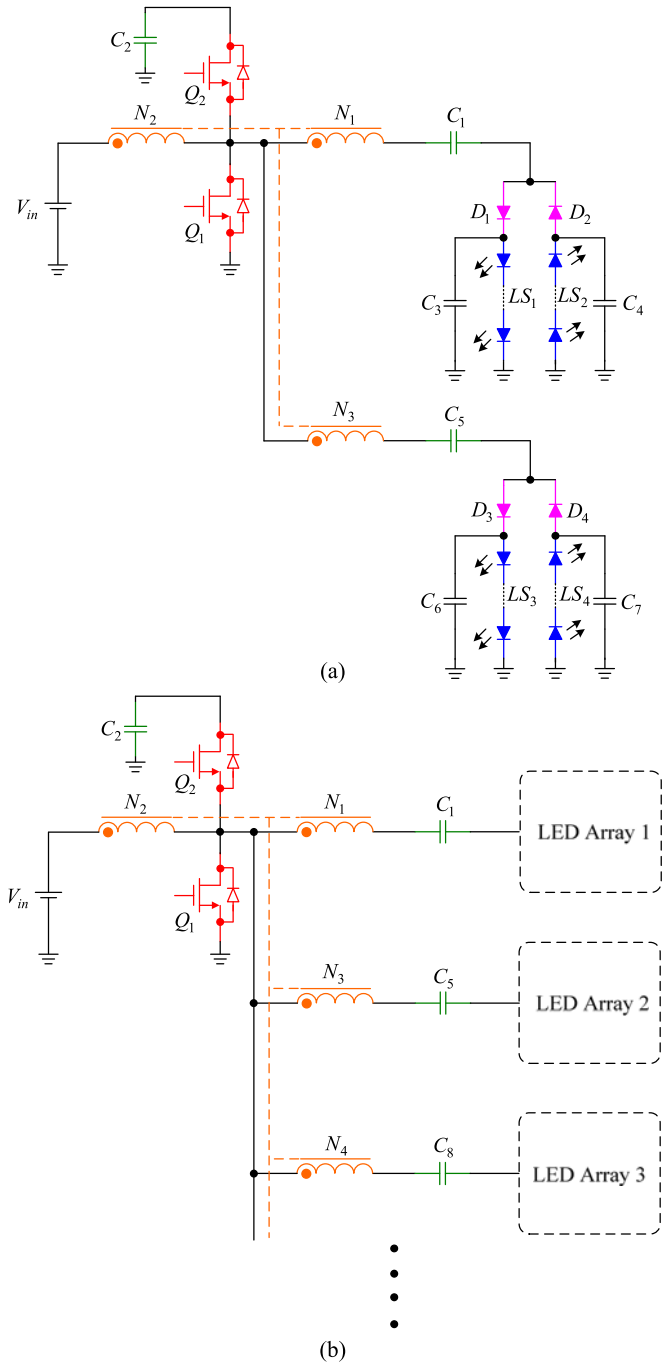

Fig. 7. Extension of the proposed two-channel LED driver: (a) four-channel LED driver, (b) multichannel LED driver.

where $V_{\text{LED},k}$, $R_{\text{LED},k}$, and $V_{F,k}$ are the total LED voltage, the total on-resistance, and the total forward voltage, respectively.

Therefore, the total LED voltages on LED strings LS_1 and LS_2 are shown as follows:

$$V_{\text{LED},k,1} = R_{\text{LED},k,1} I_{\text{LED},1} + V_{F,k,1} \tag{31}$$

$$V_{\text{LED},k,2} = R_{\text{LED},k,2} I_{\text{LED},2} + V_{F,k,2} \tag{32}$$

where $V_{\text{LED},k,1}$, $R_{\text{LED},k,1}$, $I_{\text{LED},1}$, and $V_{F,k,1}$ are the total LED voltage, total on-resistance, LED current, and total forward voltage for LS_1, respectively. $V_{\text{LED},k,2}$, $R_{\text{LED},k,2}$, $I_{\text{LED},2}$, and

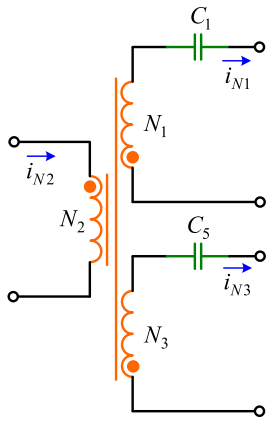

Fig. 8. Concept for analyzing multichannel current sharing.

TABLE I
SYSTEM SPECIFICATIONS OF THE PROPOSED LED DRIVER

System parameters	Specifications
Input voltage $V_{\rm in}$	$3.3\ {\rm V} \pm 10\%$
Nominal LED channel voltages $V_{\rm C3}$, $V_{\rm C4}$	$3.5\ {\rm V} \times 5 = 17.5\ {\rm V} \pm 10\%$
Nominal LED channel currents I_{o1}, I_{o2}	350 mA
Switching frequency f_s	100 kHz

$V_{F,k,2}$ are the total LED voltage, total on-resistance, LED current, and total forward voltage for LS_2, respectively.

By combining (31) and (32), the following equation can be found:

$$V_{{\rm LED},k,1} + V_{{\rm LED},k,2} = R_{{\rm LED},k,1} I_{{\rm LED},1} + V_{F,k,1} + R_{{\rm LED},k,2} I_{{\rm LED},2} + V_{F,k,2}. \quad (33)$$

From the analysis of the automatic current sharing in Section II-D, the currents in two LED strings are balanced. Thus, (33) can be expressed as

$$\begin{aligned} V_{{\rm LED},k,1} + V_{{\rm LED},k,2} &= \left(R_{{\rm LED},k,1} + R_{{\rm LED},k,2}\right) I_{{\rm LED},1} \\ &\quad + \left(V_{F,k,1} + V_{F,k,2}\right) \\ &= \left(R_{{\rm LED},k,1} + R_{{\rm LED},k,2}\right) I_{{\rm LED},2} \\ &\quad + \left(V_{F,k,1} + V_{F,k,2}\right). \end{aligned} \quad (34)$$

Next, the current in each LED string can be expressed as

$$\begin{aligned} I_{{\rm LED},1} &= I_{{\rm LED},2} \\ &= \frac{\left(V_{{\rm LED},k,1} + V_{{\rm LED},k,2}\right) - \left(V_{F,k,1} + V_{F,k,2}\right)}{R_{{\rm LED},k,1} + R_{{\rm LED},k,2}}. \end{aligned} \quad (35)$$

In (35), $V_{{\rm LED},k,1} + V_{{\rm LED},k,2}$ is the sum of the voltages across the two LED strings, equal to $V_{\rm C3} + V_{\rm C4}$ as shown in (10). Therefore, substituting (10) into (35) yields the following equation:

$$I_{{\rm LED},1} = I_{{\rm LED},2} = \frac{\frac{1+\frac{N_1}{N_2}}{1-D} \cdot V_{\rm in} - \sum V_{F,{\rm LED}}}{\sum R_{F,{\rm LED}}} \quad (36)$$

TABLE II
COMPONENTS USED IN THE PROPOSED LED DRIVER

Components		Product name
MOSFET switches	Q_1, Q_2	AON6500
Energy-transferring capacitor	C_1, C_2	$10\ \mu$F MLCC $\times$ 2
Output capacitor	C_3, C_4	$47\ \mu$F MLCC $\times$ 1
Coupled inductor		Core: KAM106060A
		N_1:N_2 = 24:6
		$L_1 = 46.4\ \mu$H, $L_{\rm lk1} = 1.4\ \mu$H
		$L_2 = 2.9\ \mu$H, $L_{\rm lk2} = 0.09\ \mu$H
		$L_m = 45\ \mu$H, $k = 0.97$
Diodes D_1, D_2		V20120C

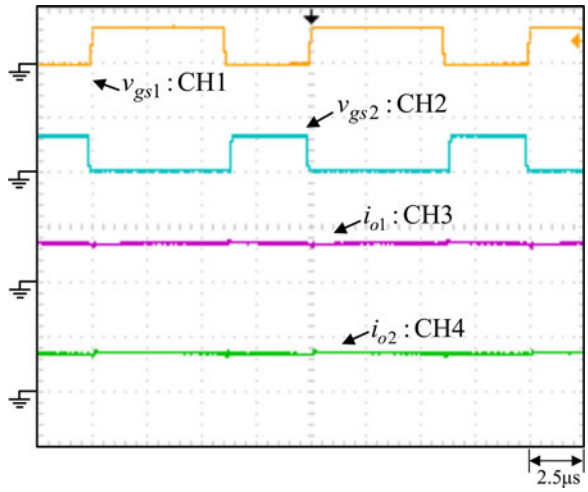

Fig. 9. Waveforms at input voltage of 3.3 V: (a) $v_{\rm gs1}$ [20V/div], (b) $v_{\rm gs2}$ [20V/div], (c) i_{o1} [500 mA/div], (d) i_{o2} [500 mA/div].

where $\sum V_{F,{\rm LED}}$ and $\sum R_{F,{\rm LED}}$ are the sum of the forward voltages and sum of the on-resistances for the two LED strings, respectively.

From (36), it can be seen that given a turns ratio, and the forward voltages and on-resistances of the LEDs, the current in each LED string can be regulated by controlling the duty cycle D, which can be achieved based on current control.

F. Extension to a Multichannel LED Driver

Based on the proposed two-channel LED driver, the two-channel LED driver can be extended to a four-channel LED driver and a multichannel LED driver as shown in Fig. 7(a) and (b), respectively. The concept of how to achieve current sharing in each LED string is illustrated in Fig. 8. From Fig. 8, all the coils are wound on the same core to form a three-winding coupled inductor and multiwinding coupled inductor, respectively. It is noted that the primary side is constructed by the coil N_2, and the secondary side is built up by the other coils. Therefore, from Fig. 8, if N_1 is equal to N_3, the currents $i_{\rm N1}$ and $i_{\rm N3}$ will be equal. Moreover, as shown in Fig. 7(a), the capacitor C_1 is used to balance the currents in the LED array 1, and the capacitor C_5 is used to balance the currents in the LED array 2. Similarly, the LED current sharing concept can be applied to the proposed LED driver with more than four LED channels as shown in Fig. 7(b).

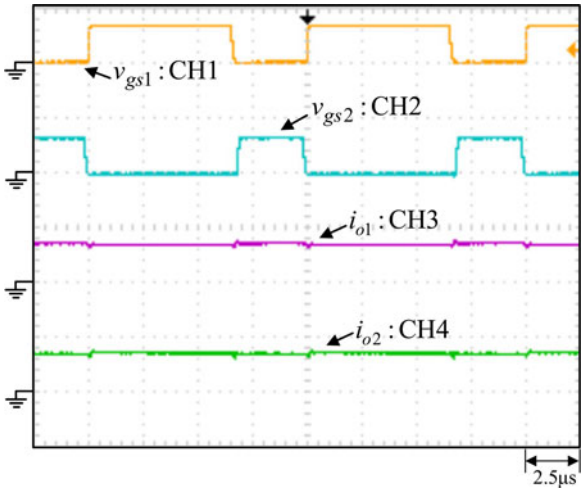

Fig. 10. Waveforms at input voltage of 2.97 V: (a) $v_{\rm gs1}$ [20V/div], (b) $v_{\rm gs2}$ [20V/div], (c) i_{o1} [500 mA/div], (d) i_{o2} [500 mA/div].

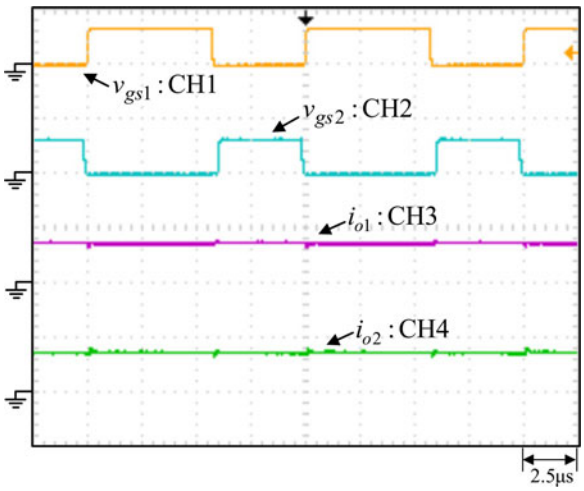

Fig. 11. Waveforms at input voltage of 3.63 V: (a) $v_{\rm gs1}$ [20V/div], (b) $v_{\rm gs2}$ [20V/div], (c) $i_{\rm o1}$ [500 mA/div], (d) i_{o2} [500 mA/div].

III. Design Considerations

To demonstrate the effectiveness of the proposed LED driver, a prototype is built and tested. Table I shows the specifications of the proposed converter, whereas, Table II shows the components used in the proposed converter. Moreover, the design procedures are described below, including the LED strings, the duty cycle, and the coupled inductor.

A. Selection of LED

The high power LEDs used for the proposed LED driver are made by Everlight Electronics, Ltd., with a product name of EHP-AX08EL/GT01H-P01/5670/Y/K42 [26]. From this datasheet, it can be seen that if the nominal constant current flowing through the LED is 350 mA, the corresponding nominal forward voltage is about 3.5 V. Besides, the variations in the LED forward voltage are $\pm 10\%$ of the nominal value. In the proposed two-channel LED driver, five LEDs are connected for each string. Therefore, the maximum voltage of the forward

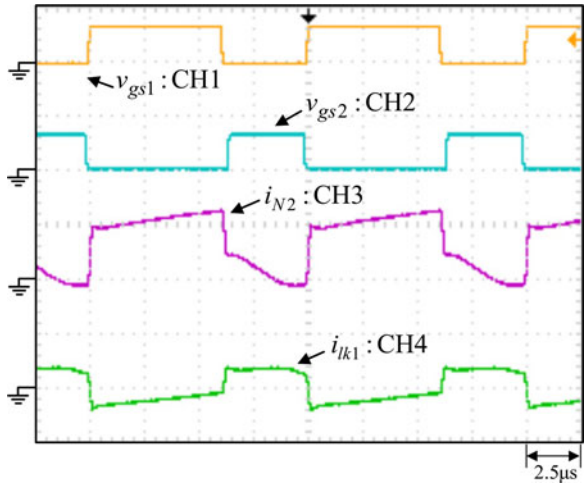

Fig. 12. Waveforms at input voltage of 3.3 V: (a) $v_{\rm gs1}$ [20V/div], (b) $v_{\rm gs2}$ [20V/div], (c) $i_{\rm N2}$ [5A/div], (d) $i_{\rm lk1}$ [2.5A/div].

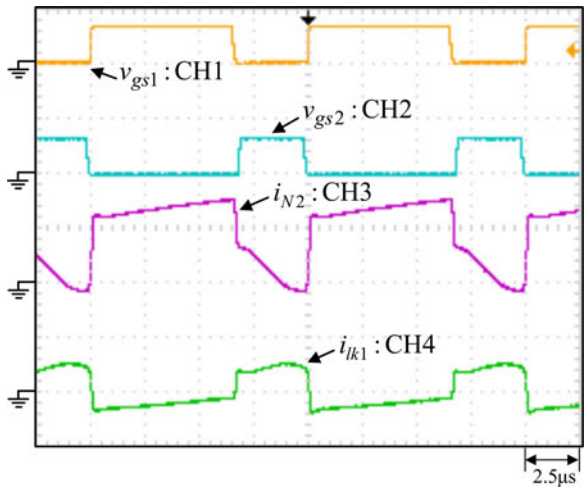

Fig. 13. Waveforms at input voltage of 2.97 V: (a) $v_{\rm gs1}$ [20V/div], (b) $v_{\rm gs2}$ [20V/div], (c) $i_{\rm N2}$ [5A/div], (d) $i_{\rm lk1}$ [2.5A/div].

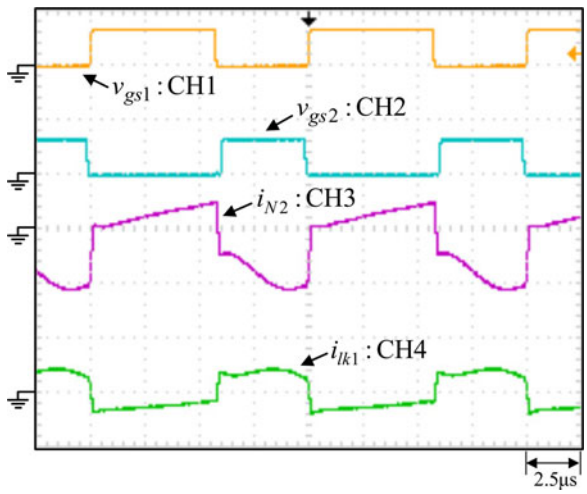

Fig. 14. Waveforms at input voltage of 3.63 V: (a) $v_{\rm gs1}$ [20V/div], (b) $v_{\rm gs2}$ [20V/div], (c) $i_{\rm N2}$ [5A/div], (d) $i_{\rm lk1}$ [2.5A/div].

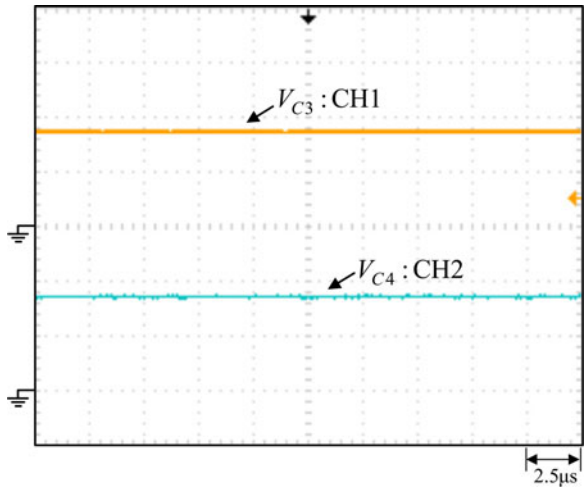

Fig. 15. Waveforms at input voltage of 3.3 V: (a) V_{C3} [10V/div], (b) V_{C4} [10V/div].

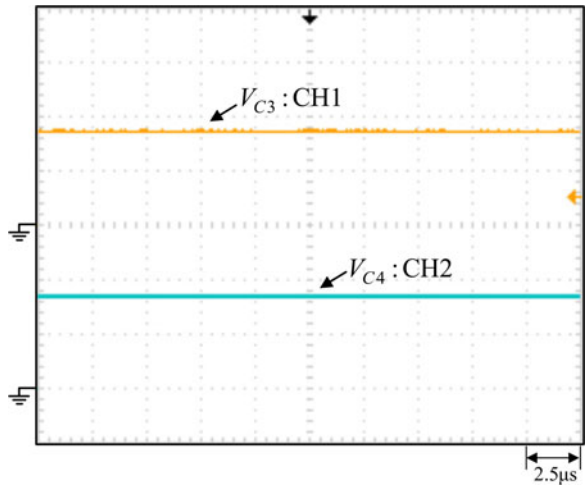

Fig. 16. Waveforms at input voltage of 2.97 V: (a) V_{C3} [10V/div], (b) V_{C4} [10V/div].

voltage for any LED channel is

$$V_{\mathrm{C3,max}} = V_{\mathrm{C4,max}} = 3.5 \times (1 + 0.1) \times 5 = 19.25\,\mathrm{V}. \quad (37)$$

Also, the minimum voltage of the forward voltage for any LED channel is

$$V_{\mathrm{C3,min}} = V_{\mathrm{C4,min}} = 3.5 \times (1 - 0.1) \times 5 = 15.75\,\mathrm{V} \quad (38)$$

where $V_{\mathrm{C3,max}}$ and $V_{\mathrm{C4,max}}$ are the maximum voltages of C_3 and C_4, respectively, and $V_{\mathrm{C3,min}}$ and $V_{\mathrm{C4,min}}$ are the minimum voltages of C_3 and C_4, respectively.

B. Determination of Duty Cycle

In the proposed LED driver, the nominal input voltage is 3.3 V with a tolerance of $\pm 10\%$. Therefore, the maximum input voltage is 3.63 V and the minimum input voltage is 2.97 V.

Since the voltage gain as shown in (9) contains the nonideal parameters of the coupled inductor, the duty cycle can be first estimated by the ideal voltage gain as shown in (10). Based on (10), the equation of the duty cycle for the proposed LED driver can be obtained as follows:

$$D = 1 - \left[\frac{V_{\mathrm{in}}}{V_{\mathrm{C3}} + V_{\mathrm{C4}}}\left(1 + \frac{N_1}{N_2}\right)\right]. \quad (39)$$

From (39), it can be seen that if the input voltage V_{in} is the minimum value and $V_{\mathrm{C3}} + V_{\mathrm{C4}}$ is the maximum value, D will be the maximum value. On the other hand, if the input voltage V_{in} is the maximum value and $V_{\mathrm{C3}} + V_{\mathrm{C4}}$ is the minimum value, D will be the minimum value. Therefore, the maximum value of D is

$$\begin{aligned} D_{\max} &= 1 - \left[\frac{V_{\mathrm{in,min}}}{V_{\mathrm{C3,max}} + V_{\mathrm{C4,max}}}\left(1 + \frac{N_1}{N_2}\right)\right] \\ &= 1 - \left[\frac{2.97}{19.25 + 19.25}(1 + 4)\right] \approx 0.6143. \end{aligned} \quad (40)$$

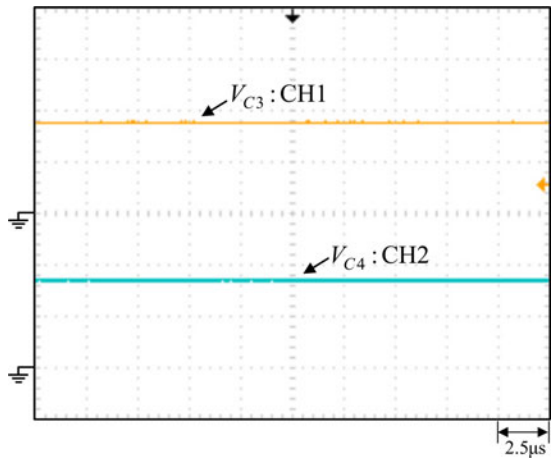

Fig. 17. Waveforms at input voltage of 3.63 V: (a) V_{C3} [10V/div], (b) V_{C4} [10V/div].

Also, the minimum value of D is

$$\begin{aligned} D_{\min} &= 1 - \left[\frac{V_{\mathrm{in,max}}}{V_{\mathrm{C3,min}} + V_{\mathrm{C4,min}}}\left(1 + \frac{N_1}{N_2}\right)\right] \\ &= 1 - \left[\frac{3.63}{15.75 + 15.75}(1 + 4)\right] \approx 0.4238 \end{aligned} \quad (41)$$

where $D_{\max}$, $D_{\min}$, $V_{\mathrm{in,max}}$ and $V_{\mathrm{in,min}}$ are the maximum duty cycle, the minimum duty cycle, the maximum input voltage, and the minimum input voltage, respectively.

C. Coupled Inductor Design

Based on (23), the maximum duty cycle shown in (40) and the minimum duty cycle shown in (41), the inequalities of the magnetizing inductance L_m can be found out as follows. From (23), it should be noted that the efficiency η will influence the magnetizing inductance L_m. If the efficiency η is higher, the magnetizing inductance L_m will be larger. Thus, the maximum magnetizing inductance occurs at $\eta = 1$. The efficiency η equal to 1 means the LED driver is lossless. Obviously, it will not be

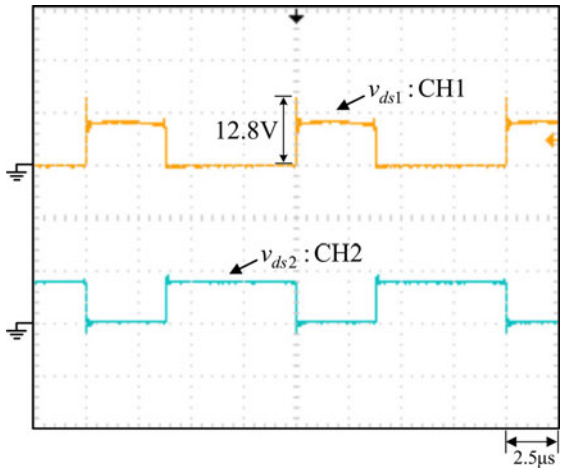

Fig. 18. Waveforms at input voltage of 3.3V: (a) $v_{\rm ds1}$ [10V/div], (b) $v_{\rm ds2}$ [10V/div].

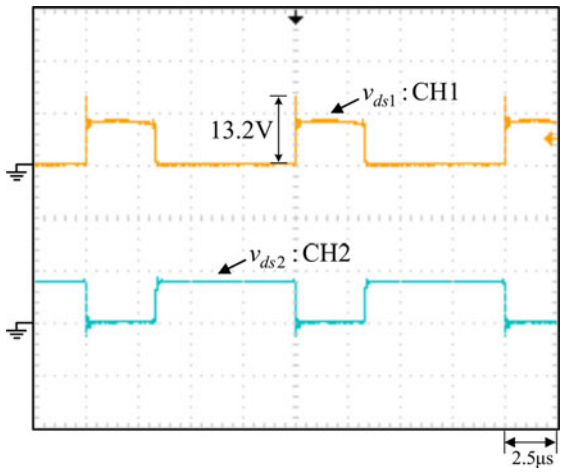

Fig. 19. Waveforms at input voltage of 2.97 V: (a) $v_{\rm ds1}$ [10V/div], (b) $v_{\rm ds2}$ [10V/div].

real. However, to obtain the maximum magnetizing inductance, the efficiency η in the following equations is set to 1.

Under the maximum input voltage and the minimum duty cycle, the accompanying inequality of $L_{\rm m}$ is

$$\begin{aligned} L_m &\geq \frac{\frac{N_1}{N_2}\cdot V_{\rm in,max}\cdot D_{\rm min}\left(1-D_{\rm min}\right)T_s\cdot\eta}{2\left(1+\frac{N_2}{N_1}\right)\cdot I_{o1}} \\ &= \frac{(4)\,(3.63)\,(0.4238)\,(1-0.4238)\,(10\mu)\,(1)}{2\left(1+\frac{1}{4}\right)(0.35)} \\ &\approx 40.5\,\mu\text{H}. \end{aligned} \tag{42}$$

Under the minimum input voltage and the maximum duty cycle, the accompanying inequality of L_m is

$$\begin{aligned} L_m &\geq \frac{\frac{N_1}{N_2}\cdot V_{\rm in,min}\cdot D_{\rm max}\left(1-D_{\rm max}\right)T_s\cdot\eta}{2\left(1+\frac{N_2}{N_1}\right)\cdot I_{o1}} \\ &= \frac{(4)\,(2.97)\,(0.6143)\,(1-0.6143)\,(10\mu)\,(1)}{2\left(1+\frac{1}{4}\right)(0.35)} \\ &\approx 32.2\ \mu\text{H}. \end{aligned} \tag{43}$$

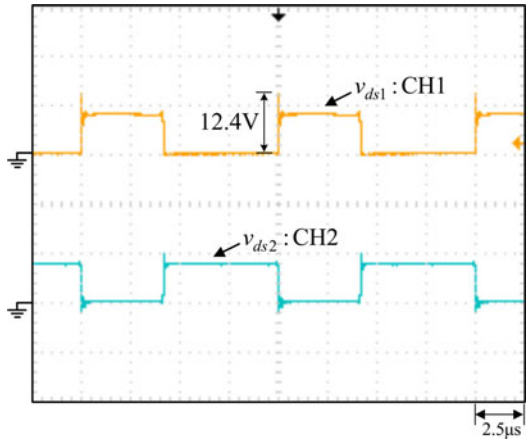

Fig. 20. Waveforms at input voltage of 3.63 V: (a) $v_{\rm ds1}$ [10V/div], (b) $v_{\rm ds2}$ [10V/div].

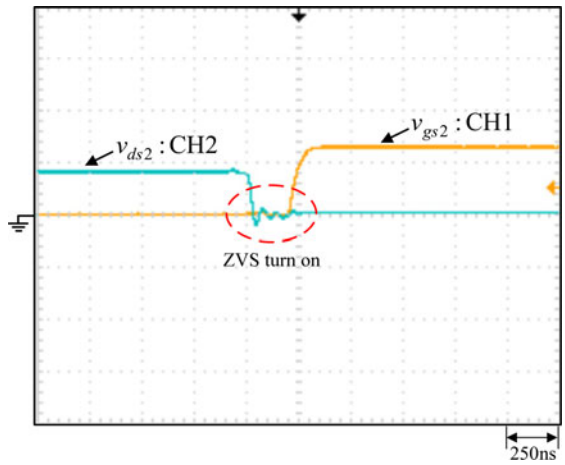

Fig. 21. Turn-on transition of Q_2 at input voltage of 3.3V: (a) $v_{\rm gs2}$ [10V/div], (b) $v_{\rm ds2}$ [10V/div].

To make sure that the magnetizing inductance L_m is always positive, the value of the magnetizing inductance should be selected larger than 40.5 μH as shown in (42). The parameters of the coupled inductor are measured to be $L_1 = 46.4\ \mu$H, $L_{\rm lk1} = 1.4\ \mu$H, $L_2 = 2.9\ \mu$H, $L_{\rm lk2} = 0.09\ \mu$H, $L_m = 45\ \mu$H, and $k = 0.97$.

IV. Experimental Results

Figs. 9 to 11 show the gate driving signals $v_{\rm gs1}$ and $v_{\rm gs2}$ for the switches Q_1 and Q_2, and the LED currents i_{o1} and i_{o2}, under three different input voltage levels of 3.3, 2.97, and 3.63 V, respectively. From Figs. 9 to 11, it can be seen that under these different input voltages, the currents in both LED strings are about 350 mA. Although under the different input voltages, the duty cycle will vary so that the currents in the both LED strings are regulated to 350 mA. Figs. 12–14 show the currents of $i_{\rm N2}$ and $i_{\rm lk1}$ under the different input voltages. From Figs. 12–14, it can be seen that the currents match the theoretical analysis. The current $i_{\rm lk1}$ has positive and negative parts. According to the principle of the ampere–second balance, the area of the positive part of $i_{\rm lk1}$ is equal to the area of the negative part of $i_{\rm lk1}$. Therefore, the currents in both LED strings

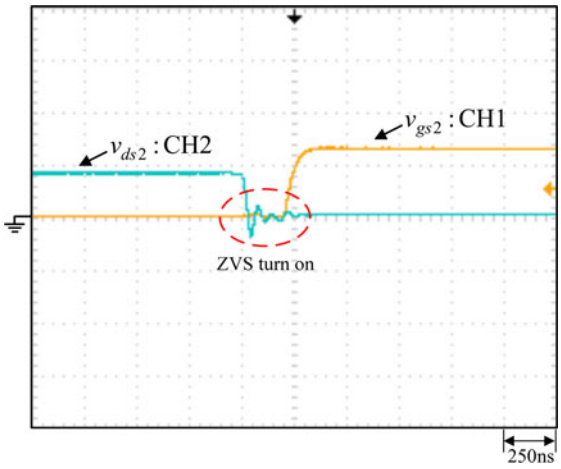

Fig. 22. Turn-on transition of Q_2 at input voltage of 2.97 V: (a) v_{gs2} [10V/div], (b) v_{ds2} [10V/div].

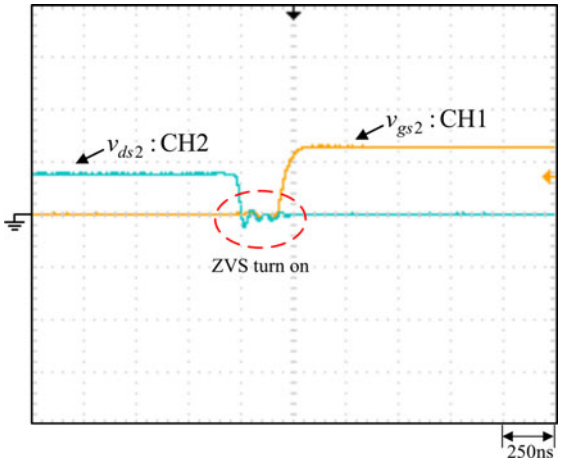

Fig. 23. Turn-on transition of Q_2 at input voltage of 3.63 V: (a) v_{gs2} [10V/div], (b) v_{ds2} [10V/div].

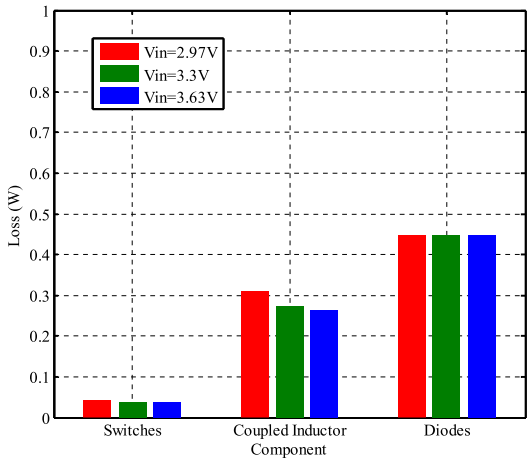

Fig. 24. Loss breakdowns of the proposed LED driver.

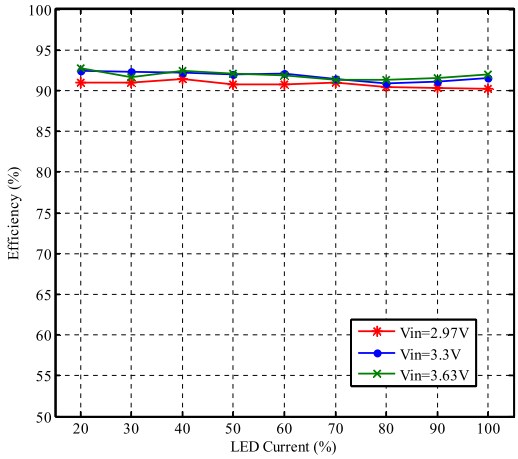

Fig. 25. Measured efficiency versus LED current.

can be balanced naturally as described in Section II-D. Figs. 15–17 show the individual voltages across the both LED strings under the different input voltages. From Figs. 15–17, it can be seen that the voltages are about 17.2 V with five LEDs used. Figs. 18–20 show the voltage stresses across Q_1 and Q_2. From Figs. 18 to 20, it can be seen that the voltage spike across Q_1 is clamped to a low value. Accordingly, the MOSFETs with low turn-on resistance can be used, so two AON6500 MOSFETs are chosen for Q_1 and Q_2, with a voltage rating of 30 V and turn-on resistance less than 0.95 mΩ. Figs. 21–23 show the turn-on transition of Q_2 under the different input voltages. From Figs. 21 to 23, it can be seen that Q_2 can achieve ZVS turn-on under the different input voltages.

Fig. 24 shows the loss breakdown analysis of the key components in the proposed topology at rated load under three input voltage levels, including switches, diodes, and a coupled inductor. First, it can be seen that when the input voltage is lower, the input current will be larger. Thus, the conduction losses of the switches will be higher. Although the switch Q_2 possesses ZVS turn-on, the switching loss from the turn-off transition of Q_2 and the turn-on and turn-off transitions of Q_1 are taken into consideration. As compared with the switching loss, the conduction loss dominates at rated load. Second, the higher the input voltage is, the higher ac flux density and hence the higher the core loss. However, the major loss comes from the conduction loss in the copper. This is because the smaller input voltage will result in higher input current. Third, the diode losses are almost equal, because the average currents of two diodes are almost equal, and hence, the conduction losses of two diodes are both almost equal. Also, from Fig. 24, it can be seen that the major power losses are from the diodes. Thus, to further improve the efficiency, the diodes with low forward voltage can be used for D_1 and D_2. Finally, Fig. 25 shows the measured curves of efficiency versus LED current, under three input voltage levels. From Fig. 25, it can be seen that the efficiencies from 20% to 100% of the rated LED current locates between 90% and 95%.

V. Conclusion

A nonisolated two-channel LED driver with automatic current balance and zero-voltage switching is presented. Based on the topology of the bidirectional converter [22], the currents in the two LED strings of the proposed LED driver can be balanced naturally without any additional active components and passive components. Since the proposed LED driver is based on the

bidirectional converter [22], its features a high step-up gain. Therefore, the turns ratio of the coupled inductor can be adjusted in design to meet the LED voltages even if a small input voltage is fed to this LED driver. In addition, the two switches can be driven by using only one half-bridge driver, so no isolated driver is required. Also, the analysis shows that the LED currents can be regulated by changing the duty cycle. Above all, the proposed nonisolated two-channel LED driver features a simple and easy design, and low cost. Furthermore, the proposed two-channel LED driver can be extended to a multichannel LED driver. Moreover, the loss breakdown analysis of the proposed LED driver shows that the major losses come from the diodes. Therefore, to further improve the efficiency, the diodes with low forward voltage can be used.

REFERENCES

[1] M. G. Craford, "LEDs challenge the incandescents," *IEEE Circuits Device Mag.*, vol. 8, no. 1, pp. 24–29, Aug. 1992.

[2] N. Narendran and Y. Gu, "Life of LED-based white light sources," *IEEE Display Technol.*, vol. 1, no. 1, pp. 167–171, Sep. 2005.

[3] K. I. Hwu and Y. T. Yau, "Applying one-comparator counter-based sampling to current sharing control of multi-channel LED strings," in *Proc. IEEE Appl. Power Electron. Conf.*, 2010, pp. 737–742.

[4] H. J. Chiu, Y. K. Lo, J. T. Chen, S. J. Cheng, C. Y. Lin, and S. C. Mou, "A high-efficiency dimmable LED driver for low-power lighting applications," *IEEE Trans. Ind. Electron.*, vol. 57, no. 2, pp. 735–743, Feb. 2010.

[5] U. Hu and M. M. Jovanovic, "LED driver with self-adaptive drive voltage," *IEEE Trans. Power Electron.*, vol. 23, no. 6, pp. 3116–3125, Nov. 2008.

[6] S. N. Li, W. X. Zhong, W. Chen, and S. Y. R. Hui, "Novel self-configurable current-mirror techniques for reducing current imbalance in parallel light emitting diode (LED) strings," *IEEE Trans. Power Electron.*, vol. 27, no. 4, pp. 2153–2162, Apr. 2012.

[7] K. I. Hwu and S. C. Chou, "A simple current balancing converter for LED lighting," in *Proc. 24th Appl. Power Electron. Conf. Expo.*, Feb. 2009, pp. 587–590.

[8] K. I. Hwu, W. C. Tu, and M. J. Hong, "A LED current balancing driver with magnetizing inductance energy recycling considered," in *Proc. 27th Appl. Power Electron. Conf. Expo.*, Feb. 2012, pp. 975–979.

[9] K. I. Hwu, W. C. Tu, and M. J. Hong, "A dimmable LED driver based on current balancing transformer with magnetizing energy recycling considered," *IEEE Display Technol.*, vol. 10, no. 5, pp. 388–395, May 2014.

[10] X. Wu, Z. Wang, and J. Zhang, "Design considerations for dual-output quasi-resonant flyback LED driver with current-sharing transformer," *IEEE Trans. Power Electron.*, vol. 28, no. 10, pp. 4820–4830, Oct. 2013.

[11] Y. L. Lin, H. J. Chiu, Y. K. Lo, and C. M. Leng, "LED backlight driver circuit with dual-mode dimming control and current-balancing design," *IEEE Trans. Ind. Electron.*, vol. 61, no. 9, pp. 4632–4639, Sep. 2014.

[12] S. M. Baddela and D. S. Zinger, "Parallel connected LEDs operated at high frequency to improve current sharing," in *Proc. IEEE 39th Conf. Rec. IAS Annu. Meet.*, 2004, pp. 1677–1681.

[13] X. K. Wu, J. M. Zhang, and M. Q. Zhao, "A simple two-channel LED driver with automatic precise current sharing," *IEEE Trans. Ind. Electron.*, vol. 58, no. 10, pp. 4783–4788, Oct. 2011.

[14] J. Zhang, L. Xu, X. Wu, and Z. Qian, "A precise passive current balancing method for multi-output LED drivers," *IEEE Trans. Power Electron.*, vol. 26, no. 8, pp. 2149–2159, Aug. 2011.

[15] C. Zhao, X. Xie, and S. Liu, "Multioutput LED drivers with precise passive current balancing," *IEEE Trans. Power Electron.*, vol. 28, no. 3, pp. 1438–1448, Mar. 2013.

[16] J. Wang, J. Zhang, X. Huang, and L. Xu, "A family of capacitive current balancing methods for multi-output LED drivers," in *Proc. 26th Annual IEEE Appl. Power Electron. Conf. Expo.*, Fort Worth, TX, USA, Mar. 6–11, 2014, pp. 2040–2046.

[17] W. Feng, F. C. Lee, and P. Mattavelli, "Optimal trajectory control of LLC resonant converters for LED PWM dimming," *IEEE Trans. Power Electron.*, vol. 29, no. 2, pp. 4820–4830, Feb. 2014.

[18] X. Wu, C. Hu, J. Zhang, and Z. Qian, "Analysis and design considerations of LLCC resonant multioutput DC/DC LED driver with charge balancing and exchanging of secondary series resonant capacitors," *IEEE Trans. Power Electron.*, vol. 30, no. 2, pp. 780–789, Feb. 2015.

[19] X. Chen, D. Huang, Q. Li, and F. C. Lee, "Multichannel LED driver with CLL resonant converter," *IEEE Trans. Emerg. Sel. Opt. Power Electron.*, vol. 3, no. 3, pp. 979–987, Sep. 2015.

[20] Y. Yu, F. Zhang, and J. Ni, "Capacitor clamped current sharing circuit for multistring LEDs," *IEEE Trans. Ind. Electron.*, vol. 61, no. 5, pp. 2423–2431, May 2014.

[21] E. E. d. S. Filho, P. H. A. Miranda, E. M. Sa, Jr., and F. L. M. Antunes, "A LED driver with switched capacitor," *IEEE Trans. Ind. App.*, vol. 50, no. 5, pp. 3046–3054, Sep./Oct. 2014.

[22] Y. T. Yau, W. Z. Jiang, and K. I. Hwu, "Bidirectional operation of high step-down converter," *IEEE Trans. Power Electron.*, vol. 30, no. 12, pp. 6829–6844, Dec. 2015.

[23] R. W. Erickson and D. Maksimovic, *Fundamentals of Power Electronics*, 2nd ed. Norwell, MA, USA: Kluwer, 2001.

[24] M. K. Kazimierczuk, *High-Frequency Magnetic Components*, 2nd ed. West Sussex, U.K.: Wiley, 2014.

[25] R.-L. Lin and Y.-F. Chen, "Equivalent circuit model of light-emitting diode for system analyses of lighting drivers," in *Proc. Conf. Rec. IEEE Ind. Appl. Soc. Annu. Meet.*, Houston, TX, USA, Oct. 4–8, 2009, pp. 1–5.

[26] (2009). [Online]. Available: http:/www.everlight.com/

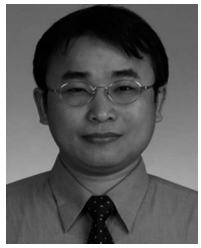

K. I. Hwu (M'06) was born in Taichung, Taiwan, on August 24, 1965. He received the B.S. and Ph.D. degrees in electrical engineering from National Tsing Hua University, Hsinchu, Taiwan, in 1995 and 2001, respectively.

From 2001 to 2002, he was the Team Leader of the Voltage-Regulated Module at AcBel Company. From 2002 to 2004, he was a Researcher at the Energy and Resources Laboratories, Industrial Technology Research Institute. He is currently a Professor at the Institute of Electrical Engineering, National Taipei University of Technology, Taipei, Taiwan, where he was the Chairman of the Center for Power Electronics Technology from 2005 to 2006. His current research interests include power electronics, converter topology, and digital control.

Dr. Hwu has been a Member of the Program Committee of the IEEE Applied Power Electronics Conference and Exposition since 2005. He has also been a Member of the Technical Review Committee of the Bureau of Standards, Metrology, and Inspection since 2005. Since 2008, he has been a Member of the IET.

W. Z. Jiang (S'12) was born in Changhua, Taiwan, on May 9, 1989. He received the B.S. and M.S. degrees in electrical engineering from National Taipei University of Technology, Taipei, Taiwan, in 2011 and 2013, respectively, where he is currently working toward the Ph.D. degree.

His research interests include power electronics and digital control.